JABFM
eISSN 2280-8000

J Appl Biomater Funct Mater 2017; 15 (Suppl 1): S45-S51
DOI: 10.5301/jabfm.5000352

ORIGINAL RESEARCH ARTICLE

Open Access

First-principles calculation of adsorption of shale gas on $CaCO_3$ (100) surfaces

Qiang Luo[1,2], Yikun Pan[2], Ping Guo[2], Zhouhua Wang[2], Na Wei[2], Pengfei Sun[1], Yuxiao Liu[1]

[1] School of Science, Southwest Petroleum University, Chengdu - PR China
[2] State Key Laboratory of Oil and Gas Reservoir Geology and Exploitation, Southwest Petroleum University, Chengdu - PR China

ABSTRACT

Background: To demonstrate the adsorption strength of shale gas to calcium carbonate in shale matrix, the adsorption of shale gas on $CaCO_3$ (100) surfaces was studied using the first-principles method, which is based on the density functional theory (DFT).

Methods: The structures and electronic properties of CH_4, C_2H_6, CO_2 and N_2 molecules were calculated by the generalized gradient approximation (GGA), for a coverage of 1 monolayer (ML). Under the same conditions, the density of states (DOS) of $CaCO_3$ (100) surfaces before and after the adsorption of shale gas molecules at high-symmetry adsorption sites were compared.

Results: The results showed that the adsorption energies of CH_4, C_2H_6, CO_2 and N_2 on $CaCO_3$ (100) surfaces were between 0.2683 eV and -0.7388 eV. When a CH_4 molecule was adsorbed at a hollow site and its 2 hydrogen atoms were parallel to the long diagonal (H3) on the $CaCO_3$ (100) surface, it had the most stable adsorption, and the adsorption energy was only -0.4160 eV. The change of adsorption energy of CH_4 was no more than 0.0535 eV. Compared with the DOS distribution of CH_4 before adsorption, it shifted to the left overall after adsorption. At the same time, the partial density of states (PDOS) curves of $CaCO_3$ (100) surfaces before and after adsorption basically overlapped.

Conclusions: This work showed that the adsorption effect of shale gas on calcium carbonate is very weak, and the adsorption is physisorption at the molecular level.

Keywords: Adsorption energy, $CaCO_3$ (100) surface, First-principles, Shale gas

Introduction

Shale gas, as one of the global unconventional natural gases, has received extensive attention around the world. The United States and Canada have achieved commercial exploitation of shale gas with good results. China has done a lot of work with respect to shale gas research status, reservoiring mechanisms and favorable-area evaluation, but the study of the adsorption of shale gas was only just initiated in recent years (1, 2). The development from conventional oil and gas fields to shale gas fields actually reflects the scale transition from micron to nanometer, and macroscopic breakthroughs have become increasingly dependent on microscopic studies. Therefore, it becomes particularly important to improve our microscopic understanding by using new theories and methods (3). Moreover, the study of shale gas molecule adsorption on shale substrate surfaces helps to understand the occurrence of shale gas, to assess the gas adsorption capacity quantitatively, to explore the correlation of adsorption properties and mineral composition and to evaluate the quantity of shale gas as a natural resource.

Shale gas is generally dry and mainly consists of CH_4, C_2H_6, CO_2, N_2 and other components, with the content of CH_4 up to more than 95% (4, 5). The adsorption of shale gas and shale has been investigated through a large number of experimental and theoretical studies (6-12). Most of the theoretical studies show that shale gas is mainly absorbed on the surface of the kerogen and clay minerals, and is almost not adsorbed at all on the surface of calcium carbonate (13-16). Ji et al (5) studied methane adsorption on clay minerals of different sources and origins by isothermal adsorption experiment. The results showed that different types of clay minerals had evidently different gas adsorption capacities. However, there is no direct evidence of very weak gas adsorption on the surface of calcium carbonate.

Accepted: March 17, 2017
Published online: May 29, 2017

Corresponding author:
Prof. Ping Guo
State Key Laboratory of Oil and Gas
Reservoir Geology and Exploitation
Southwest Petroleum University
No. 8 Xindu Avenue
Xindu District, Chengdu, PR China
guopingswpi@vip.sina.com

At the same time, the first-principles method is used to study the adsorption of gas molecules on material surface (17-26), but there are few reports about the adsorption of gas molecules on the surface of calcium carbonate. Based on density functional theory with solid-state nuclear magnetic resonance (SS-NMR) calculations, Bevilaqua et al (27) simulated the adsorption of hydrocarbon molecules on calcite surface ($CaCO_3(10\bar{1}4)$), but the adsorption of shale gas was not studied. In this paper, we adopted the first-principles method based on density functional theory (DFT) to study the adsorption stability of shale gas and its components at different high-symmetry positions on $CaCO_3$ (100) surfaces. By analyzing the adsorption results, such as the adsorption energy of gas molecules and the structure and electronic properties of $CaCO_3$ (100) surfaces, we uncovered the microscopic mechanisms of shale gas adsorption on $CaCO_3$ surfaces.

Methods

Computational methods

Based on the first-principle method of DFT (28, 29), the ground state geometries and electronic properties of CH_4, C_2H_6, CO_2 and N_2 molecules adsorbed on $CaCO_3$ (100) were calculated using the Cambridge Sequential Total Energy Package (CASTEP) module in Materials Studio. Within the generalized gradient approximation (GGA), Perdew-Burke-Ernzerhof (PBE) (30) exchange correlation functionals combined with ultrasoft pseudopotentials were used in the calculations. The value of plane wave cutoff energy was 300 eV. The K point grid (31) size was 3 × 1 × 1. Self-consistent field calculations were performed with a convergence criterion of 2.0×10^{-6} eV on single atom energy. The convergence of parameters was tested for each supercell. The Broyden-Fletcher-Goldfarb-Shanno (BFGS) optimization algorithm proposed by Broyden, was used in the structure optimization (32-35).

Structural models

In this paper, the P (1 × 1) periodic supercell is used as the initial surface. Under the coverage of 1 monolayer (ML), the adsorption of CH_4, C_2H_6, CO_2 and N_2 on the surface was theoretically studied for each. First, an optimized $CaCO_3$ unit cell (Fig. 1) was cleaved for a (100) surface. Then a vacuum layer of 2-nm thickness was constructed to simulate the $CaCO_3$ (100) surface (Fig. 2). Finally, the $CaCO_3$ (100) structure was optimized. We focused on shale gas molecule adsorption on $CaCO_3$ (100) surfaces. Therefore, in the structural optimization computation, the position of oxygen atoms was kept on the surface layer, and the number of adsorbed of shale gas molecules was variable, whereas the atoms of the non–surface layer were immobilized. We adopted such a setting to simulate the adsorption of $CaCO_3$ on shale gas molecules in order to reduce the number of calculations and to exclude the effect of substrate thickness. The initial lattice constant of calcium carbonate was an experimental value for, a = 0.499 nm, c = 1.7061 nm (36). After optimization, the lattice constant was a = 0.499 nm, c = 1.7060 nm. The gas molecules were added on the $CaCO_3$ (100) surface to a height of 0.5 nm.

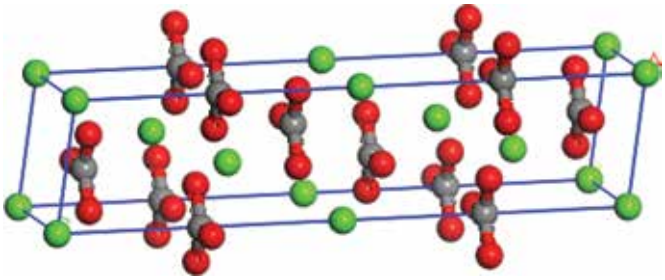

Fig. 1 - Structural model of an optimized $CaCO_3$ cell with oxygen atoms (red), calcium atoms (green) and carbon atoms (gray).

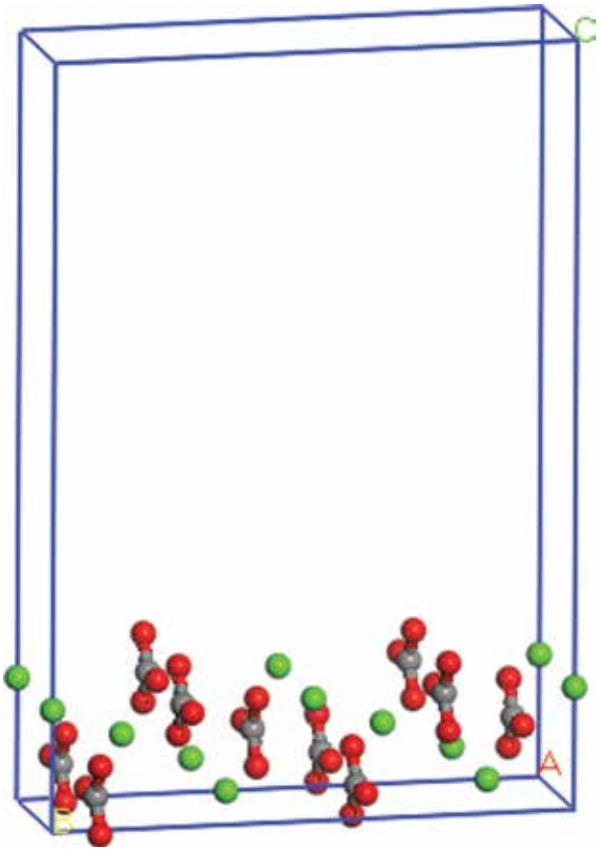

Fig. 2 - Structural model of a $CaCO_3$ (100) surface supercell with vacuum layer.

In the structural model of $CaCO_3$ (100) surface supercell, there were 3 possible high-symmetry adsorption sites, the top (T), the bridge (B) and the hollow (H) part, in a parallelogram consisting of 4 oxygen atoms of surface (Fig. 3). The bridges included the short-side bridge (B1) and the long-side bridge (B2).

Due to the nature of parallelogram geometry, each gas molecule had 4 types of adsorption forms in the $CaCO_3$ (100) surface H site. As shown in Figure 4, H1 was parallel to the short edge of the parallelogram, H2 was parallel to the short diagonal, H3 was parallel to the long diagonal and H4 was parallel to the long edge. Similarly, T-type sites were denoted

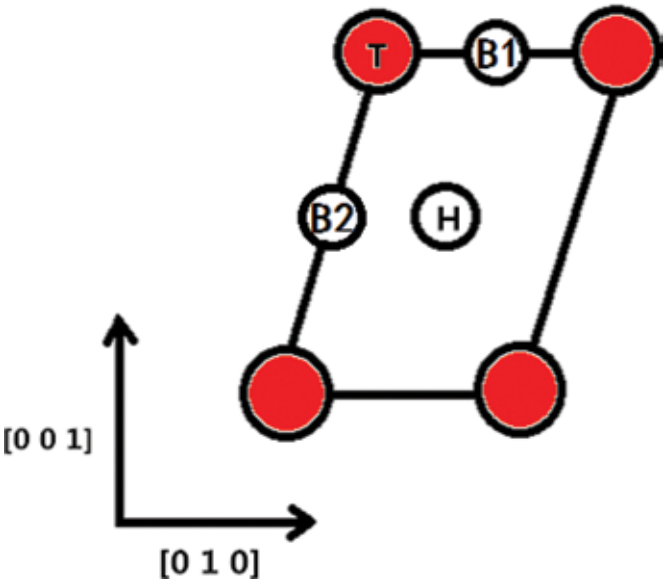

Fig. 3 - High-symmetry adsorption site on p (1 × 1) $CaCO_3$ (100) surface: top (T), short-side bridge (B1), long-side bridge (B2) and hollow (H).

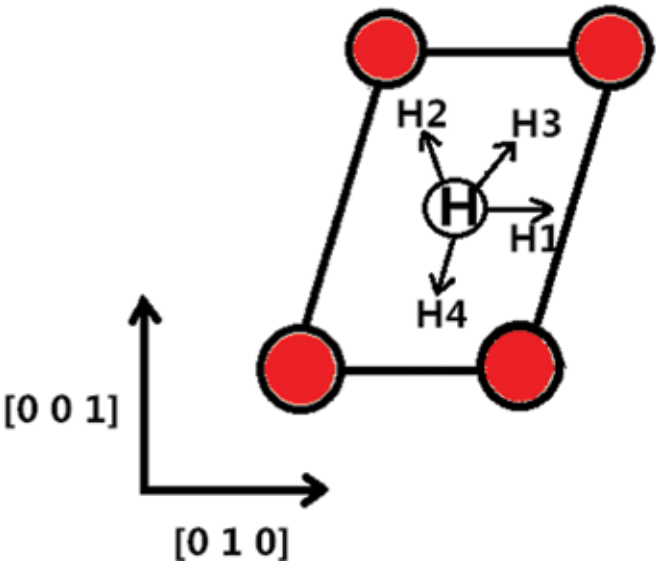

Fig. 4 - Adsorption directions of H site.

by T1, T2, T3 and T4, and B-type sites were mainly related to the situation in which the adsorption of gas molecules was parallel to the short edge or long edge, and were designated as B11, B14, B21 and B24. Therefore, taking all of the possibilities into account, each gas species of CH_4, C_2H_6, CO_2 and N_2 had 12 adsorption modes on the $CaCO_3$ (100) surface.

To analyze the adsorption stability of shale gas molecules on $CaCO_3$ (100) surfaces, the adsorption energy of gas molecules on $CaCO_3$ (100) surfaces was calculated. The total energy of the system before adsorption was obtained by calculating the energy of $CaCO_3$ (100) surfaces and gas molecules. Then in the same way, the total energy of the system was calculated after adsorption. The equation to calculate the adsorption energy is given by

$$\Delta E_{ad} = E_{gas+CaCO_3} - (E_{CaCO_3} + E_{gas}) \quad \text{Eq. [1]}$$

where $E_{gas+CaCO3}$ is the total energy of the system after gas adsorption, E_{CaCO3} is the energy of pure $CaCO_3$ without the gas molecule, and E_{gas} is the energy of the isolated shale gas molecule. The value of ΔE_{ad} reflects the stability of the adsorption system. $\Delta E_{ad} < 0$ means that the energy of the system decreases after adsorption, and the gas molecules are adsorbed. The adsorption process is exothermic. $\Delta E_{ad} > 0$ means that the energy of the system increases, and the gas molecules cannot be adsorbed (37). A smaller value of ΔE_{ad} indicates better stability of the adsorption system.

Results and discussion

Analysis of adsorption energy

Table I lists the adsorption energy of CH_4, C_2H_6, CO_2 and N_2 molecules on $CaCO_3$ (100) surfaces in the 12 adsorption modes. CH_4, C_2H_6 and N_2 molecules had negative ΔE_{ad}, and the lowest adsorption energy was -0.4160 eV, -0.7388 eV and -0.1567 eV, respectively. The adsorption capacity of 3 kinds of

TABLE I - Adsorption energy of CH_4, C_2H_6, CO_2 and N_2 molecules on 12 types of adsorption sites on $CaCO_3$ (100) surfaces

High-symmetry sites	Adsorption energy (eV)			
	CH_4	C_2H_6	CO_2	N_2
T1	-0.3886	-0.7087	0.1872	-0.0855
T2	-0.3625	-0.6933	0.1463	-0.1567
T3	-0.3676	-0.7260	0.1619	-0.1505
T4	-0.3855	-0.7022	0.1871	-0.1032
B11	-0.3967	-0.7382	0.1672	-0.0903
B14	-0.3721	-0.7388	0.2044	-0.1279
B21	-0.4034	-0.6370	0.1679	-0.0805
B24	-0.4085	-0.6211	0.2683	-0.1243
H1	-0.4080	-0.6214	0.1361	-0.0971
H2	-0.4107	-0.6849	0.1521	-0.1363
H3	-0.4160	-0.6592	0.1127	-0.1312
H4	-0.4137	-0.6286	0.2033	-0.1195

T1 = on the top site and parallel to the short edge of the parallelogram; T2 = on the top site and parallel to the short diagonal; T3 = on the top site and parallel to the long diagonal; T4 = on the top site and parallel to the long edge; B11 = on the short side bridge site and parallel to the short edge; B14 = on the short-side bridge site and parallel to the long edge; B21 = on the long-side bridge site and parallel to the short edge; B24 = on the long-side bridge site and parallel to the long edge; H1 = on the hollow site and parallel to the short edge of the parallelogram; H2 = on the hollow site and parallel to the short diagonal; H3 = on the hollow site and parallel to the long diagonal; H4 = on the hollow site and parallel to the long edge.

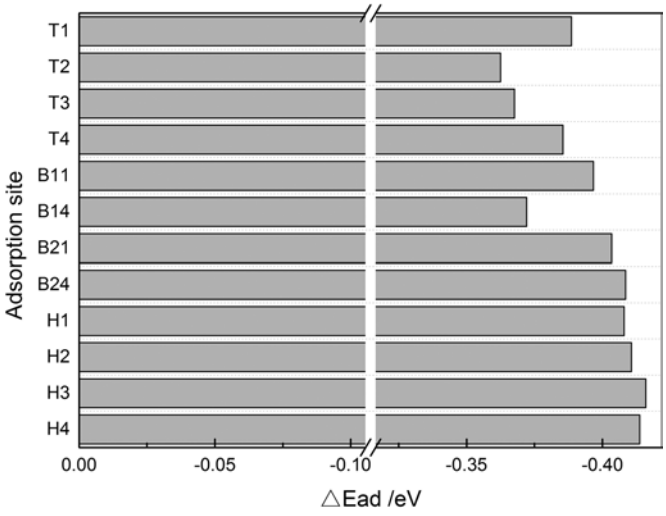

Fig. 5 - Bar chart of adsorption energy of CH_4 at various adsorption sites on the $CaCO_3$ (100) surface.

gases on the surface of calcium carbonate follows the order of C_2H_6 > CH_4 > N_2. However, the ΔE_{ad} of CO_2 was positive, which means that CO_2 molecule cannot be adsorbed on the surface of calcium carbonate. Therefore, the adsorption of CO_2 is not discussed in the following.

Since the percentage of CH_4 is dominant in shale gas, the adsorption energy of CH_4 molecular was compared for different adsorption sites to analyze the stability of shale gas molecules adsorbed on $CaCO_3$ (100) surfaces, as shown in Figure 5. It can be seen that CH_4 molecules had the lowest ΔE_{ad} at the H3 site.

From the point of view of the quantity of adsorption energy, CH_4 molecules had a minimum adsorption energy of -0.4160 eV on H3, which was the most stable adsorption structure among the 12 high-symmetry sites (Fig. 6). Therefore, it is relatively easier for CH_4 molecules to be adsorbed on H3. When adsorbed on T2, CH_4 molecules had a maximum energy of -0.3625 eV, which means that it was most difficult for T2 to adsorb CH_4 molecules. Similarly, C_2H_6 molecules had their minimum adsorption energy and most stable adsorption structure at B14, which was the position for easiest adsorption. B24 had the maximum energy and the most unstable adsorption structure. At T2, N_2 molecules had their minimum adsorption energy, and could be easily adsorbed at T2. B21 was the most difficult position to adsorb N_2 molecules. The small absolute values of adsorption energy indicate very weak adsorption of CH_4, C_2H_6 and N_2 molecules on $CaCO_3$ (100) surfaces.

In terms of the range of adsorption energies, the adsorption energy of CH_4 at different sites ranged from -0.3625 eV to -0.4160 eV, with the largest difference being only 0.0535 eV. Besides, the largest differences of the adsorption energy ranges for C_2H_6 and N_2 molecules were only 0.1177 eV and 0.0762 eV, respectively. The range of adsorption energies was very small, which indicates that the adsorption of each gas molecule at the high-symmetry sites on $CaCO_3$ (100) surfaces was very similar, and the gas molecules tended to move on the calcium carbonate surfaces. By comparison, it is known that the mobility of CH_4 is the strongest.

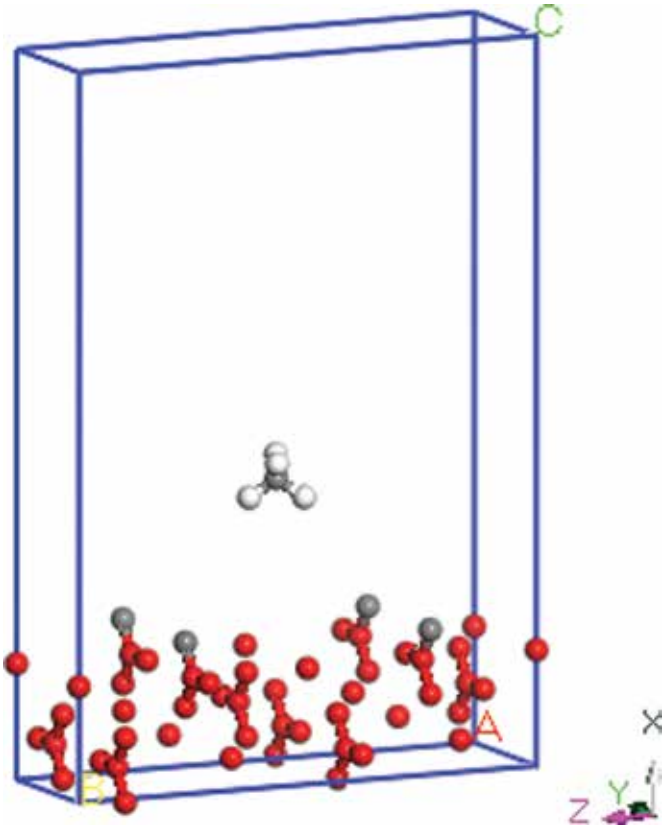

Fig. 6 - Structural model of CH_4 molecule adsorbed at H3 site on $CaCO_3$ (100) surface.

Analysis of physical structure

In Table II, we can see that after CH_4 molecules were adsorbed at H3 sites, the C-H bond length became 0.1097 nm, which is in good agreement with the experimentally spectroscopic data of 0.1086 ± 0.0001 nm (38). Compared with the value before adsorption, the bond length changed by 0.091%, and bond angle changed by 0.779%.

Similarly, the physical structure was analyzed for C_2H_6 and N_2 before and after adsorption. The relative changes were 1.422% and 1.400% for C=C bond length and H-C-H bond angle of C_2H_6, respectively. The N≡N bond length increased by 1.396% after N_2 was adsorbed. It was found that the structures of CH_4, C_2H_6 and N_2 molecules showed negligible changes, so the adsorption effect was weak on the $CaCO_3$ (100) surface.

Analysis of density of states

The CASTEP module can analyze the band structure, electronic density of states (DOS), optical properties, phonon dispersion relations, phonon DOS and stress before and after the optimization of the physical model. Here we mainly discuss the electronic DOS changes and their effect on adsorption. According to the analysis of the DOS changes for CH_4, C_2H_6, N_2 and $CaCO_3$ (100) surfaces before and after adsorption, the interactions between shale gas molecules and $CaCO_3$ (100) surface can be further understood.

TABLE II - Changes of bond length and bond angle of CH_4, C_2H_6 and N_2 molecules on $CaCO_3$ (100) surfaces after adsorption

Gas type	Before adsorption		After adsorption*		Relative change	
	Bond length† (nm)	Bond angle‡ (°)	Bond length (nm)	Bond angle (°)	Bond length	Bond angle
CH_4	0.1098	109.483	0.1097	110.336	0.091%	0.779%
C_2H_6	0.1547	109.471	0.1525	107.938	1.422%	1.400%
N_2	0.1146	180	0.1162	180	1.396%	0

* Situation for the most stable adsorption position.
† The bond lengths were C-H for CH_4, C = C for C_2H_6, N ≡ N for N_2.
‡ The bond angles were C-H for CH_4 and C_2H_6, N ≡ N for N_2.

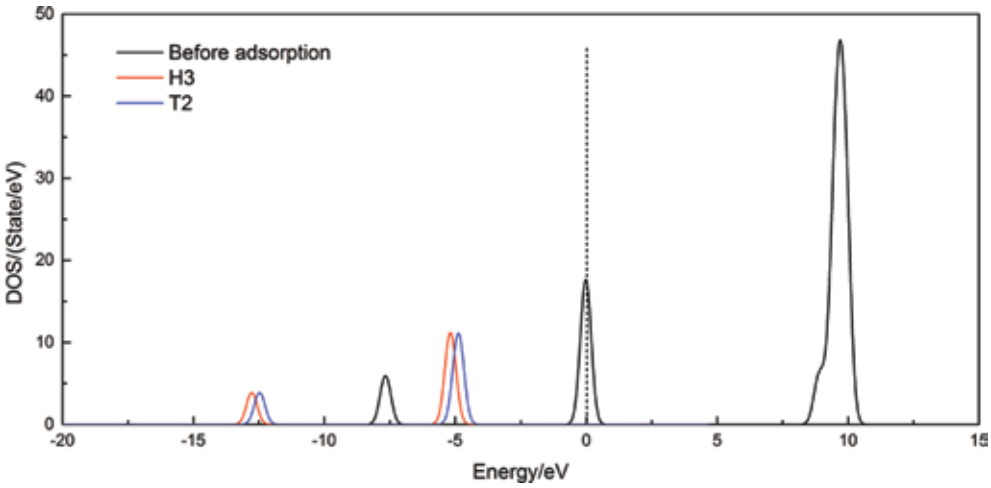

Fig. 7 - Density of states (DOS) of CH_4 molecules before and after adsorption at H3 site and T2 site. The black dotted line indicates the Fermi level.

In Figure 7, the DOS of CH_4 before and after adsorption at H3 and T2 is compared. The black curve represents the electronic DOS before adsorption, the red curve represents the electronic DOS after adsorption at H3, and the blue curve represents the electronic DOS after adsorption at T2. The vertical dashed line at 0 eV indicates the Fermi level. It can be seen that whether adsorbed at H3 or T2, the electron DOS curves of CH_4 molecules shifted to the left overall after adsorption. The adsorption energy decreased, and the electronic structure became more stable, which shows that the adsorption had a significant influence on the distribution of electron DOS of CH_4 molecules. Besides, the DOS curve of H3 has 2 peaks, at -12.77 eV and -5.18 eV, which move to the left about 0.3 eV compared with those of T2 at -12.47 eV and -4.88 eV. It is thus proven that the adsorption of CH_4 molecules on $CaCO_3$ (100) surface high-symmetry sites is basically from the point of view of electronic structure, and has better mobility on the surface of the calcium carbonate.

Figure 8 shows the partial density of states (PDOS) of oxygen atoms in $CaCO_3$ (100) surface before and after the adsorption of CH_4 molecules at H3 under the coverage of 1 ML. The contribution of *s* electronic states and *p* electronic states to the total density of states in energy regions is different. When the energy is greater than -10 eV, the *p* electronic states (red curve) play a major role in the total electron density. When the energy is less than -10 eV, the *s* electronic states (blue curve) play a major role in the total electron density. Before adsorption, the *s* electronic states energy is mainly continuously distributed in the ranges of 0 eV to -9 eV and -17 eV to -24 eV, and there are 7 peaks in the 2 intervals. While *p* electronic states energy is mainly continuously distributed in the ranges of 2 eV to -9 eV and -17 eV to -24 eV, and there are 9 peaks in the 2 intervals. After adsorption, the PDOS of *s* electronic state of oxygen atoms basically coincides with that of the state before adsorption, as does that of the *p* Electronic State. This suggests that there is no chemical bond formed between CH_4 molecules and the oxygen atoms on $CaCO_3$ (100) surfaces. This indicates that the adsorption of CH_4 on calcium carbonate surfaces is mainly affected by the Van Der Waals force, and it is physical adsorption. To better illustrate this point, we compared the DOS of $CaCO_3$ (100) surfaces with the different shale gas molecules adsorbed, as shown in Figure 9.

Figure 9 presents the DOS of CH_4, C_2H_6 and N_2 adsorbed on a $CaCO_3$ (100) surface. We can see that the adsorption of different gas molecules on the $CaCO_3$ (100) surface has similar effects on the electronic structure of the oxygen atom on the $CaCO_3$ (100) surface. After adsorption, the 3 DOS curves almost overlap, indicating that C_2H_6 and N_2 molecules have similar adsorption effects on oxygen atoms on the $CaCO_3$ (100) surface to those of the CH_4 molecule, and the adsorption of the 3 kinds of gas molecules on the $CaCO_3$ (100) surface are physical.

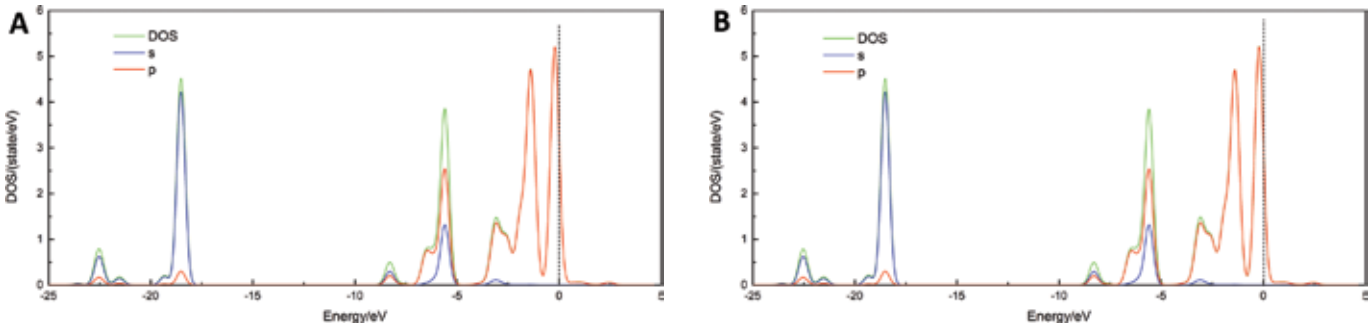

Fig. 8 - Partial density of states (PDOS) and density of states (DOS) of oxygen atoms in $CaCO_3$ (100) surface before and after the adsorption of CH_4 molecules on the H3 site. (**A**) Before adsorption and (**B**) after adsorption.

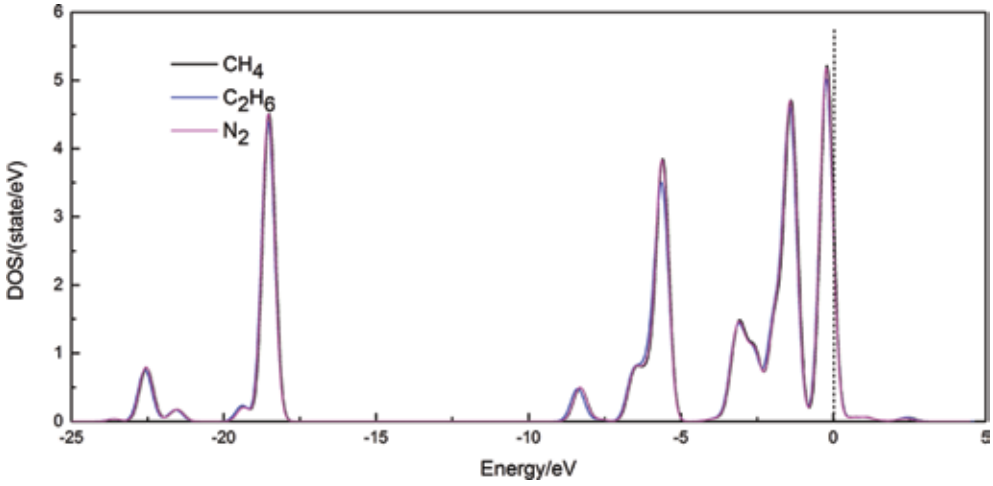

Fig. 9 - Density of states (DOS) of oxygen atoms on $CaCO_3$ (100) surface after the adsorption of CH_4, C_2H_6 and N_2 molecules at the most stable adsorption sites.

Conclusions

Using the first-principle method based on DFT, we established adsorption models for CH_4, C_2H_6, CO_2 and N_2 on $CaCO_3$ (100) surfaces, and calculated the corresponding adsorption energies. The adsorption abilities of CH_4, C_2H_6 and N_2 molecules on the $CaCO_3$ (100) surface were weak. CO_2 molecules could not be adsorbed. The adsorption abilities of the different molecules were different. The adsorption ability of hydrocarbon gas was stronger than that of nonhydrocarbon gas, and the adsorption ability of C_2H_6 was stronger than that of CH_4. In addition, the adsorption energy of different gas molecules varied over the range of sites and followed the order of CH_4 <N_2 < C_2H_6. The change of CH_4 was the smallest, indicating the best mobility of CH_4 molecules on the surface of calcium carbonate. This may be due to the fact that the methane molecule has the smallest relative molecular mass.

We also analyzed the electronic structures of the adsorption systems. After adsorption, the changes of geometric structures of the molecules were small and the electron DOS of atoms in the $CaCO_3$ (100) surface was basically unchanged. The findings above show that the adsorption of shale gas molecules on the surface of calcium carbonate is physical.

Acknowledgements

The authors would like to acknowledge the assistance of A.P. Li P. Chen for English correction.

Disclosures

Financial support: This work was supported by the Young Scientists Fund of the National Natural Science Foundation of China (grant no. 51204141), the Major Program of the National Natural Science Foundation of China (grant no. 51374179), the Southwest Petroleum University Foundation (grant no. 2014QHS009, 2015JXYJ-07) and the Open Research Fund of the Computational Physics Key Laboratory of Sichuan Province (grant no. JSWL2014KF03).
Conflict of interest: The authors declare they have no conflicts of interest.

References

1. Kong DT, Ning ZF, Yang F, He B, Zhao TY. The characteristic of adsorption on shales and influence factor. Petrochem Ind Appl. 2013;32(9):1-4.
2. Ma YL, Zhang DL. Research status of shale reservoir adsorption mechanism and its influencing factors. Ground Water. 2014;36(6):246-249.
3. Gao LF, Wang QQ, Yin S, Zheng LH, Wang YY, Li H. Research of shale gas' absorption. Sichuan Univ Arts Sci J. 2014;24(2): 60-64.
4. Zeng QS, Chen WK, Dai WX, Zhang YF, Li Y, Guo X. Density functional theory study of CO and O_2 adsorption on NiFeB2/TiO_2 surface. Chin J Catal. 2010;31(4):423-428.
5. Ji LM, Qiu JL, Zhang TW, Xia YQ. Experiments on methane adsorption of common clay minerals in shale. Earth Sci J Chin Univ Geosci. 2012;37(5):1043-1050.

6. Luo XP, Wu P, Zhao JH, Yang N. Study advances on organic pores in organic matter-rich mud shale. J Chengdu Univ Technol. 2015;42(1):50-59.
7. Zhang H, Zhu YM, Xia XH, Hu L, Chen J. Comparison and explanation of the absorptivity of organic matters and clay minerals in shales. J Chin Coal Soc. 2013;38(5):812-816.
8. Zhang XF, Lu CX, Zhang LY, Liu Q. Occurrences of shale gas and their petroleum geological significance. Adv Earth Sci. 2010; 25(6):597-604.
9. Huang MZ. The quantitative characterization of containing gas abilities in shale with different occurrence states: a case study of Shuangyang formation in Yitong Basin. Sci Technol Eng. 2015;15(20):35-41.
10. Wang R, Zhang NS, Liu XJ, Wu XM, Yan J. Research progress of mechanism of adsorption and desorption of gas in shale. Sci Technol Eng. 2013;13(19):5561-5567.
11. Qajar A, Daigle H, Prodanović M. Methane dual-site adsorption in organic-rich shale-gas and coalbed systems. Int J Coal Geol. 2015;149:1-8.
12. Fathi E, Akkutlu YI. Multi-component gas transport and adsorption effects during CO_2 injection and enhanced shale gas recovery. Int J Coal Geol. 2014;123:52-61.
13. Curtis JB. Fractured shale-gas systems. AAPG Bull. 2002;86(11): 1921-1938.
14. Montgomery SL, Jarvie DM, Bowker KA, Pollastro RM. Mississippian Barnett shale, Fort Worth basin, north-central Texas: gas-shale play with multi-trillion cubic foot potential. AAPG Bull. 2005;89(2):155-175.
15. Chalmers GRL, Bustin RM. The organic matter distribution and methane capacity of the Lower Cretaceous strata of Northeastern British Columbia, Canada. Int J Coal Geol. 2007;70(1-3): 223-239.
16. Ross DJK, Bustin RM. Shale gas potential of the Lower Jurassic Gordondale Member, northeastern British Columbia, Canada. Bull Can Pet Geol. 2007;55(1):51-75.
17. Yan CX, Jiang QW. Effects of atmospheric species and vacancy defect on electron transfer between diamond (001) surface and adlayer. Eur Phys J Appl Phys. 2012;59(1):11303.
18. Kuang XJ, Wang XQ, Liu GB. A density functional theory study of carbon monoxide adsorption on platinum-doped gold clusters. Eur Phys J Appl Phys. 2012;60(3):31301.
19. Luo Q, Tang B, Zhang Z, Ran ZL. First principles calculation of adsorption for H2S on Fe (100) surface. Acta Phys Sin. 2013;62(7):077101.
20. He YB, Jia JF, Wu HS. First-principles study of stability and electronic structure of N2H4 adsorption on NiFe (111) alloy surface. Acta Phys Sin. 2015;64(20):203101.
21. Brunsvold AL, Garton DJ, Minton TK, Troya D, Schatz GC. Crossed beams and theoretical studies of the dynamics of hyperthermal collisions between Ar and ethane. J Chem Phys. 2004;121(23):11702-11714.
22. Nave S, Tiwari AK, Jackson B. Methane dissociation and adsorption on Ni(111), Pt(111), Ni(100), Pt(100), and Pt(110)-(1 × 2): energetic study. J Chem Phys. 2010;132(5):054705.
23. Li P, Liu ZZ, Liu HX, Liu DS, Ge XW. Density functional theory study of methane adsorption on Ni (110). J Inner Mongolia Norm Univ. 2015;44(3):389-395.
24. Atta-Fynn R, Ray AK. A first principles study of the adsorption and dissociation of CO_2 on the δ–Pu (111) surface. Eur Phys J B. 2009;70(2):171-184.
25. Li L, Cockayne E, Williamson I, Espinal L, Wong-Ng W. First-principles studies of carbon dioxide adsorption in cryptomelane/hollandite-type manganese dioxide. Chem Phys Lett. 2013; 580:120-125.
26. Jiao Y, Du AJ, Zhu ZH, Rudolph V, Simth SC. Adsorption of carbon dioxide and nitrogen on single-layer aluminum nitride nanostructures studied by density functional theory. J Phys Chem C. 2010;114(17):7846-7849.
27. Bevilaqua RC, Rigo VA, Veríssimo-Alves M, Miranda CR. NMR characterization of hydrocarbon adsorption on calcite surfaces: a first principles study. J Chem Phys. 2014;141(20):204705.
28. Hohenberg P, Kohn W. Inhomogeneous electron gas. Phys Rev. 1964;136(3B):B864-B871.
29. Kohn W, Sham LJ. Self-consistent equations including exchange and correlation effects. Phys Rev. 1965;140(4A): 1133-1138.
30. Perdew JP, Burke K, Ernzerhof M. Generalized gradient approximation made simple. Phys Rev Lett. 1996;77(18):3865-3868.
31. Monkhorst HJ, Pack JD. Special points for Brillouin-zone integrations. Phys Rev B. 1976;13(12):5188-5192.
32. Broyden CG. The convergence of a class of double-rank minimization algorithms 1: general considerations. J Inst Math Appl. 1970;6(1):76-90.
33. Fletcher R. A new approach to variable metric algorithms. Comput J. 1970;13(3):317-322.
34. Goldfarb D. A family of variable-metric methods derived by variational means. Math Comput. 1970;24(109):23-26.
35. Shanno DF. Conditioning of quasi-Newton methods for function minimization. Math Comput. 1970;24(111):647-656.
36. Graf DL. Crystallographic tables for the rhombohedral carbonates. Am Mineral. 1961;46(11):1283-1316.
37. Zhang H, Liu SY, Zhang GY, eds. Landscape painting the chemisorption of quantum mechanics. Beijing, China: Science Press; 2004;215-217.
38. Hammer B, Hansen LB, Norskov JK. Improved adsorption energetics within density-functional theory using revised Perdew-Burke-Ernzerhof functional. Phys Rev B. 1999;59(11): 7413-7421.